UNIVERSITI TEKNOLOGI MARA

MATHEMATICS LETTERS
https://sites.google.com/tmsk.uitm.edu.my/mathematicsletters

Octagon Structuring Element for Breast Tumour Classifications

[1, *]Siti Salmah Yasiran, [2] Suhaila Abd Halim &
[3] Nur Ainna Hazwani Zaidi
[1,2]Centre of Mathematical Sciences, Faculty of Computer and Mathematical Sciences, Universiti Teknologi MARA, 40450 Shah Alam, Selangor. Malaysia.
[*1]salmahyasiran@uitm.edu.my
[2]suhaila889@uitm.edu.my
[3] 2023861884@student.uitm.edu.my,
*Corresponding author

Received: 5/10/2026 Revised: 20/10/2026 Accepted: 25/10/2026 Published: 31/10/2026

ABSTRACT

Breast cancer is a health concern that affects women greatly in the global world, and the only solution to improving the survival rates is early detection of this cancer. Mammograms are a procedure that is common among the physicians during screening. These images may be difficult to interpret because of the presence of blurred or obscured information with the effect of thick breast tissue. This research examines the application of an image processing tool known as an octagon structuring element to assist a computer-aided diagnosis (CADx) system to make accurate decisions whether a tumor is benign or malignant. The data used in the research were taken from the Mini Mammography Image Analysis Society (MIAS) database as the primary source of data. The mammogram images were pre-processed by using median filters and histogram stretching to remove noise and enhance contrast, respectively. This was followed by the segmentation of the images using a modified Otsu thresholding technique to detect the important sections of the breast. To capture local features in the images, BRISK keypoints were then employed to obtain features and identify them in the images. Data were then reduced in terms of dimension with Principal Component Analysis (PCA), before the classification phase. Support Vector Machine (SVM) was utilized in refining the data to be used in the final classification. The results of the research found that the most effective octagon size was at a radius of 48. Among the 9 radii with high accuracy performance, radius 48 was chosen as the optimal level because it offers the best balance between short training time and fast prediction speed. With this radius, the system managed to achieve an accuracy of 97.60% with PCA. Then, 99.96% sensitivity, 94.39% specificity, a Dice Coefficient of 0.9789, and a Jaccard Index of 0.9586. This proves that the use of the octagon shape is very helpful in improving the quality of medical images, as well as facilitating medical experts to make more accurate and faster diagnoses.

Keywords: breast tissue classification, mathematical morphology support vector machine, structuring element.

INTRODUCTION

Breast cancer has caused 670,000 deaths and 2.3 million women being diagnosed with the disease. It occurs in almost every country and can affect women at any age after puberty, though the risk increases as they get older (World Health Organization, 2025). Breast cancer is also the second most common cancer in women and remains a leading cause of death worldwide (Trayes & Cokenakes, 2021). According to American Cancer Society (2022), breast cancer happens when abnormal cells in the breast tissue divide without control, often forming a lump or tumor. Most cases start in the milk-producing glands (lobules) or the ducts that carry milk to the nipple. Because of this, breast cancer is a major health challenge that needs a strong focus on early detection and treatment. Finding and diagnosing the cancer early can greatly improve survival rates, as early-stage breast cancer has a survival rate of over 80% (World Health Organization, 2025).

As Obeagu & Obeagu (2024) suggest the predisposing factors that promote breast cancer are BRCA (BReast CAncer) gene mutations, age, and lifestyle. BRCA mutations refer to the mutations of BRCA1 or BRCA2 tumor suppressor genes. In developed nations, it has been found that screening is more commonly used to achieve early diagnosis whereas symptoms such as a breast lump or nipple discharge are more commonly seen in patients from poorer nations. Diagnosis is usually done by carrying out mammograms, physical examination and biopsies. It should be noted that benign tumors are non-cancerous and remain in a single location whereas malignant tumors are fast and spread. Making early detection essential for effective treatment and improved recovery outcomes (Aljuaid et al., 2022).

To increase survival rates and treatment opportunities, early detection of breast cancer is very important. There are two main ways to find breast cancer which are checking for symptoms like lumps or testing people who show no signs of the disease (Barrios, 2022). According to American Cancer Society (2023), women aged 55 and over can choose to continue with annual mammograms or have mammograms every two years.While women aged 40-45 have the option to start annual mammogram screening, women aged 45-54 need to have mammograms. In addition, additional imaging such as magnetic resonance imaging (MRI) is used to increase the accuracy of diagnosis for BRCA gene mutation carriers. Finding breast lesions is hard even for experienced doctors because small or unclear details can lead to mistakes or a wrong diagnosis (Loizidou et al., 2023).

To assist in the breast cancer diagnosis process, computer-aided diagnosis (CAD) technology has begun to be used, and it is a valuable tool in breast imaging. The main benefit of CAD is that it helps reduce the number of missed cancer cases and overlooked spots by helping doctors find small or unclear tumors in mammograms that might be hard to see (Heine et al., 2021; Yasiran et al., 2020a). Subsequently, computer-aided diagnosis (CADx) is being developed, which plays a role in detecting and classifying lesions into benign or malignant categories using machine learning methods. In CAD and CADx systems, morphological image processing is an important technique for extracting important features from mammogram images. One of the best tools for this is the usage of structural elements (SE), which studies the structure and form of tissues.

This research indicates that mathematical morphology is a highly helpful stage in the preparation of mammogram images prior to analysis (Loizidou et al., 2023). This technique assists in making images sharper by removing noise and emphasizing valuable information required to detect breast cancer. It works well at preserving original shapes of the tissue and is typically applied to things such as filtering and detecting edges (Sun et al., 2022). These extracted features can be highlighted by machine learning algorithms, enhancing the classification of benign and malignant tumors (Yasiran et al., 2020a). The Support Vector Machine (SVM) algorithm functions on the principle of locating the optimal hyperplane between two or more categories and may be extended to it through the assistance of morphological features (Shubham & Kamalraj, 2022). Machine learning has also been applied to enhance the detection and diagnosis of breast cancer and with the addition of mathematical morphology, the effectiveness of CAD systems is enhanced.

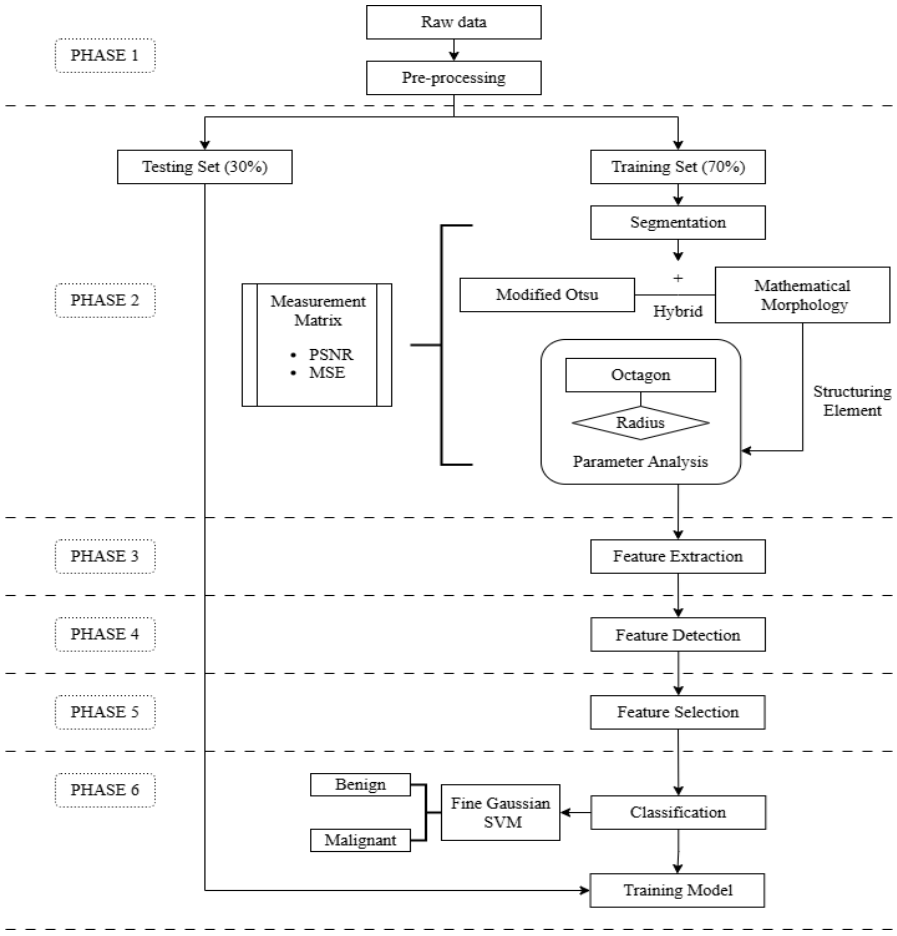
THE PROPOSED METHOD

Proposed Framework

Figure 1 illustrates the research methodology and the overall process that includes the six phases involved in conducting this research.

Figure 1

Flowchart of the Proposed Study



Phase 1: Preprocessing

The first phase begins with preprocessing, where raw images are turned into a more suitable form for further analysis. Image preprocessing is an important basic step to reduce complexity and improve image quality by using several techniques in an automatic breast cancer detection system using computer technology. If this process is continued without preprocessing, artifacts in the image will make it difficult to segment accurately. To obtain a clean image quality, techniques such as resizing, noise reduction, normalization, and contrast enhancement are used (Soliman et al., 2021). Preprocessing is especially important for medical images like mammograms. Because these images are detailed and complex, they need to be processed first to ensure the results are more reliable and easier for physicians to understand. The methods of filtering, as one of the main ways of preprocessing mammogram images. According to Avcı & Karakaya (2023), are applied to mammogram images with the goal of achieving the

better quality of the image and a higher value of segmentation. The MIAS images were preprocessed using median filtering and histogram stretching in this research. A median filter operates as a nonlinear digital filtering technique that reduces noise while maintaining essential image features like edges. It is particularly efficient in reducing salt-and-pepper noise and speckle noise, making it suitable for mammogram enhancement (Hemali et al., 2023).

Phase 2: Segmentation

The second phase continues with image segmentation, where this process divides an image into several parts or segments, each of which represents meaningful areas in the image by considering pixel characteristics. The main goal of segmentation is to change the image into a format that is easier to understand and study (Islam et al., 2024). While there are many algorithms available, such as K-means++ clustering and the Modified Watershed Algorithm. This research chooses to use Modified Otsu's thresholding because it is efficient and simple that proposed by (Yasiran et al., 2020b). This method focuses only on the background and foreground data. It automatically finds the best threshold by making the difference between pixel groups as large as possible, while keeping the differences within each group as small as possible (Khairnar et al., 2021; Yasiran et al., 2020a, 2020b). The formula for determining the threshold value at which the total of the background and foreground is at its lowest,

$$\sigma_{\omega}^{2}(Q) = \sum_{j=0}^{Q=1} \rho(j).\sigma_{\beta}^{2} + \sum_{j=0}^{N-1} \rho(j) + \sigma_{\omega}^{2}\,(Q) \tag{1}$$

The corresponding between-class variance is obtained from the total and within-class variance, as stated in Equation 2, while Equation 3 expresses the between-class variance in terms of the background and foreground class means.

$$\sigma_{\psi}^{2}(Q) = \sigma^{2}(Q) - \sigma_{\varsigma}^{2}(Q) \tag{2}$$

$$\sigma_{\psi}^{2}(Q) = \sum_{j=0}^{Q=1} \rho(j).[m_{\beta}(Q) - m]^{2} + \sum_{j=0}^{N-1} \rho(j).[m_{\omega}(Q) - m]^{2} \tag{3}$$

The modified Otsu formulation replaces the mean-based quantity used in the original formulation with a standard-deviation-based term. The standard deviation is defined in Equation 4, and the modified between-class expression is given in Equation 5.

$$SD = \sqrt{\frac{\sum_{j=0}^{N}(k_j - \check{\mathrm{K}})^2}{N}} \tag{4}$$

$$\sigma_{\psi}^{2}(Q) = \sum_{j=0}^{Q=1} \rho(j).\sum_{j=0}^{N-1} \rho(j).[SD_{\beta} - SD_{\omega}]^{2} \tag{5}$$

The threshold selected from this formulation was then used before mathematical morphology.

Mathematical Morphology and Octagon Structuring Element

Mathematical morphology (MM) was applied after thresholding to refine the segmented image. Although erosion and dilation represent the two fundamental morphological operations, the segmentation procedure in this study specifically employed the erosion operator. Let A denote the image set, and B denote the corresponding structuring element (SE). The erosion and dilation operations are defined in Equations 6 and 7, respectively.

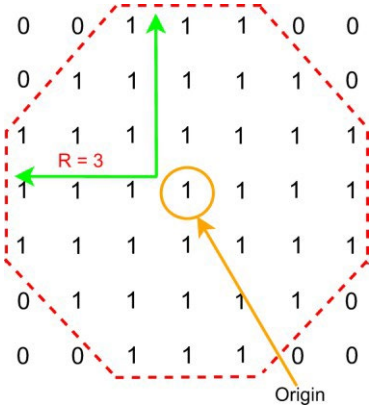
$$A \ominus B = \{G|(B)_z \subseteq A\}, A, B \in G^2 \quad (6)$$

$$A \oplus B = \{G|(B)_z \cap A \neq \emptyset\}, A, B \in G^2 \quad (7)$$

The octagon structuring element is a type of flat binary mask used in morphological operations like dilation and erosion. It is a 2D shape that provides a balance between a square and a disk. It is more isotropic than a square, but the calculation is easier than a disk. Its use is also suitable for processing images that have natural features or round structures, such as in medical applications or object imaging. Also, the octagon structuring element is typically characterized by the radius parameter, r. The r indicates dimension and is the distance from the origin of the structuring element to the sides of the octagon measured along the horizontal and vertical effective axes. The parameter r must be a non-negative factor of 3, as this constraint is a built-in requirement of MATLAB's morphological structuring element. Besides that, MATLAB offers a unique structure that directly creates octagon-shaped structuring element, which can be conveniently used in image analysis. Figure 2 shows the octagon shaped structuring elements. In MATLAB commands, octagon structuring element can be constructed using the syntax: SE = strel("octagon", r); where, r = The distance from the structuring element origin to the sides of the octagon.

Figure 2

Octagon-shaped Structuring Element



Phase 3 & Phase 4: Feature Extraction and Feature Detection

The Binary Robust Invariant Scalable Keypoints (BRISK) algorithm was created to detect image forgery and object recognition based on the multi-scale angular feature. The algorithm is based on the calculation of key points of a scaled image, which is usually corners or edges, and building a binary descriptor around them. BRISK is based on a fixed sampling pattern of concentric rings to sample and match intensities of pixels. In the case where the value of the first point in a pair is more than the second, then a binary value (1 or 0) is assigned. Once these keypoints have been identified, matching similar areas in images is the last phase and it must be done in a quick and effective way. (Leutenegger et al., 2011).

Phase 5: Feature Selection

The Principal Component Analysis (PCA) was used to indicate the differences and the main patterns in the dataset. PCA generates the first components which are the principal components, and which capture the greatest variation of the data. In this study, the PCA was also utilized to reduce the dimensional of the data to eliminate redundancies. Kaosain Akbar (2022).

Phase 6: Classification

The Support Vector Machine (SVM) is an effective machine learning algorithm in the classification phase. SVM functions to identify the optimal hyperplane that can separate two or more classes in the feature space by maximizing the margin between the data points closest to the hyperplane known as support vectors. Subsequently, separation with this maximum margin not only helps reduce classification errors but also improves the generalization ability of the model. In this study, SVM was utilized to classify between benign and malignant tumor.

ANALYSIS AND RESULTS

For this study, 70% of the data will be utilized for training, while the remaining 30% will be used for testing. The BRISK feature extraction was used to perform the analysis of the parameter of the SVM classifier with and without PCA. The analysis was divided into two parts as follows:

Analysis 1: Results of the Optimal Radius Octagon SE

Table 1

Results of the Octagon SE for Training Dataset

Radius	Accuracy (%)		AUC	Sensitivity (%)	Specificity (%)	Dice Coefficient	Jaccard Index
	Without PCA	With PCA					
3	97.4	97.6	0.9985	99.96	94.39	0.9789	0.9586
6	88.4	88.5	0.9735	99.0	77.31	0.8984	0.8156
9	88.4	88.5	0.9735	99.0	77.31	0.8984	0.8156
12	88.4	88.5	0.9735	99.0	77.31	0.8984	0.8156
27	88.4	88.5	0.9735	99.0	77.31	0.8984	0.8156
30	97.4	97.6	0.9985	99.96	94.39	0.9789	0.9586
48	97.4	97.6	0.9985	99.96	94.39	0.9789	0.9586
60	97.4	97.6	0.9985	99.96	94.39	0.9789	0.9586
72	97.4	97.6	0.9985	99.96	94.39	0.9789	0.9586
81	88.4	88.5	0.9735	99.0	77.31	0.8984	0.8156
90	97.4	97.6	0.9985	99.96	94.39	0.9789	0.9586
99	97.4	97.6	0.9985	99.96	94.39	0.9789	0.9586
120	88.4	88.5	0.9735	99.0	77.31	0.8984	0.8156

Table 4 shows the performance of the SVM classifier in terms of classification performance using various radius values. The findings suggest that there are two large performance groups on the radii. In the mid-range radii of 6 to 27, the accuracy is dropped to an average of 88.50% with PCA while 88.40% without PCA. On the other hand, seven radii, 3, 30, 48, 60, 72, 90, and 99, have a high result in all evaluation metrics. The accuracy of these radii is 97.6% with PCA while 96.40% without PCA. Their AUC is 0.9985 which means that this classifier can distinguish between the classes almost perfectly. The Dice coefficient (0.9789) and Jaccard index (0.9586) scores from the confusion matrix also remain high, showing strong agreement between the predicted and actual class labels. The consistency of the performance of the classifier with a range of radii suggests that the classifier is at the saturation stage so that adding and removing a radius to set does not affect the accuracy. Since the results of all the seven radii provide the same top results, it is impossible to identify an optimum radius using only the values presented in Table 1. The accuracy initially assumes high level at radius 3 and the sharply declines as the radius moves to the values in the mid-range (6, 9, 12, and 27). However, as the radius increases further beyond 30, the accuracy rises back to the maximum level and remains stable

across several radius values. This produces a noticeable "plateau" in the graph, in which the radii between 30 and 99 give near equal accuracy with PCA and without PCA conditions. Since multiple radii achieve the same highest accuracy, accuracy alone is not sufficient to identify a single optimal radius. Hence, the analysis further measures computational performance. Table 2 shows the training time and prediction speed of each of the radii to determine the radii that offers the best efficiency and also maintains the highest possible accuracy.

Table 2

Computational performance of the top-performing radii (Training)

Radius	Training Time (sec)	Prediction Speed (obs/sec)
3	13.557	4567
30	11.916	4333
48	8.149	5433
60	13.209	4233
72	21.020	2967
90	10.661	4933
99	11.527	5267

From Table 2, radius 48 shows the greatest computing performance among these radii. It records the fastest training time (8.149 seconds) and the highest prediction speed (5433 observations per second). Overall, radius 48 offers the most optimal balance between accuracy and computational efficiency, making it the most suitable choice for system performance. Among all radii tested, radius 48 provides the fastest training time and the highest prediction speed, making the most efficient option for this research. Based on this outcome, radius 48 is selected as the optimal setting for the subsequent testing processes. Table 3 shows the results for both training and testing with a radius of 48, comparing results with and without PCA.

Table 3

The performance for both Training and Testing Dataset

Dataset	Radius	Accuracy (%)		AUC	Sensitivity (%)	Specificity (%)	Dice Coefficient	Jaccard Index
		Without PCA	With PCA					
Training	48	97.4	97.6	0.9985	99.96	94.39	0.9789	0.9586
Testing	48	96.1	96.1	1	91.81	99.83	0.9563	0.9163

Based on Table 2, the utilization of PCA produced a slight improvement in model performance. Both configurations had high classification accuracy. The testing accuracy of 96.1% and training accuracy of 97.6% achieved in this research are significantly higher than the 85.9% accuracy reported by Yasiran et al., (2020) who used a disk structuring element. This improvement suggests that the octagon of radius 48 structuring element used here is more effective at capturing tumor shapes compared to the disk shape. In this case, the achieved AUC values of 0.9985 and 1 for training and testing respectively indicate excellent separation between classes. The sensitivity was quite high which implied that the model was able to detect the tumor regions. Meanwhile, the specificity values (94.39 % for training and 99.83 % for testing) confirmed that non-tumor regions were also correctly classified with minimal false positives. The Dice coefficient (0.9789 for training and 0.9563 for testing) and Jaccard index (0.9586 and 0.9163).

Analysis 2: Results of the Quality of the Mammogram Images

The mean square error (MSE) and peak signal-to-noise ratio (PSNR) were obtained in this research to measure image quality based on the previous findings. The performance evaluation of the octagon structuring element with various radii was first conducted during the training phase to determine the optimal configuration. Based on the classification performance evaluation, the best results in the training were achieved with a radius of 48. The optimal radius determined during training was subsequently evaluated using MSE and PSNR on the testing dataset. PSNR was obtained by comparing the segmented output image with the original grayscale image. The segmented result contains the detected lesion boundary. PSNR measures how much distortion is introduced by this segmentation process. A higher PSNR indicates that the segmented image is more like the original image and preserves more structural information. The PSNR and MSE values for the benign (Table 4) and malignant (Table 5) testing sets was used to evaluate the image quality after the segmentation process. PSNR measures the signal to the image noise ratio, which has a value in decibels (dB).

Table 4

PSNR and MSE values for the testing set of benign

Id Image	PSNR	MSE
mdb204	-	-
mdb207	-	-
mdb214	33.0425	32.2724
mdb218	-	-
mdb219	38.7676	8.6361
mdb222	-	-
mdb223_1	44.4068	2.3572
mdb223_2	45.0545	2.0306
mdb227	-	-
mdb236	42.9089	3.3281
mdb240	45.0162	2.0486
mdb244	45.0162	2.0486
mdb252	-	-
mdb290	-	-
mdb312	32.2360	38.8579
mdb314	-	-
mdb315	48.5126	0.9158

Table 5

PSNR and MSE values for the testing set of malignant

Id Image	PSNR	MSE
mdb223_2	45.0545	2.0306
mdb231	-	-
mdb238	-	-
mdb239_1	-	-
mdb241	48.5490	0.9082
mdb249_1	-	-
mdb249_2	-	-
mdb253	-	-
mdb256	-	-
mdb264	44.7070	2.1998

mdb267	-	-
mdb270	-	-
mdb271	-	-
mdb274	-	-
mdb293_2	43.1973	3.1142

From Table 4 and Table 5, image mdb315 from the benign set and image mdb241 from the malignant set produced the best segmentation quality, as indicated by their high PSNR values and low MSE values. The image with the highest overall quality is mdb241 of the malignant set with highest PSNR (48.5490 dB) and lowest MSE (0.9082) slightly better than the best benign image, mdb315 (PSNR 48.5126 dB, MSE 0.9148). The images marked with "-" indicate that no lesion boundary was detected after the erosion process. This happens when the structuring element is too large for certain lesion sizes, causing the segmented region to be completely removed. As a result, the segmented image becomes identical to the original image and the PSNR and MSE values are undefined.

CONCLUSION

The optimization of the radius values of octagon structuring element can lead to the improvement of the performance of the computer-aided diagnosis (CADx) systems of breast cancer in general. The performance of these systems can be enhanced by defining the advantages of employing various values of the structuring element in the classification process. The misclassification rates could be lower by a more comprehensive preprocessing policy which will enable the patients to be given the proper treatment. This contributes meaningful improvements to clinical workflows and expands current knowledge on the role of geometric morphology in medical imaging. When the octagon SE were adjusted to the values of their radius, the efficiency of the proposed CADx system has significantly increased. The experiment was able to determine the radius arrangement that had the most improvement of other tested radius, which was the best radius, R=48. With PCA, the system attained 97.60% accuracy, 99.96% sensitivity, 94.39% specificity, Dice Coefficient of 0.9789 and Jaccard Index of 0.9586 by demonstrating strong model stability in various radius settings. The PSNR and MSE evaluation showed that images that are processed with optimal radius maintained the important structural information with a minimal distortion. This is reflected in the high PSNR and low MSE values obtained for several benign and malignant images. Among the evaluated samples, image mdb241 from the malignant set and mdb315 from the benign set produced the best segmentation quality. Overall, optimizing octagon SE radii contributes meaningfully to achieving accurate, efficient, and robust breast tumor classification. These results show the potential of the proposed CADx system for early and reliable breast cancer detection and the significance of morphological parameter optimization.

ACKNOWLEDGEMENT

The authors would like to acknowledge Universiti Teknologi MARA (UiTM) and Faculty of Mathematical and Computer Sciences (FSKM) for their support and contributions.

Conflict of Interest
The authors have no conflicts of interest to declare.

Non-funded
This research received no specific grant from any funding agency in the public, commercial, or not-for-profit sectors.

REFERENCES

Aljuaid, H., Alturki, N., Alsubaie, N., Cavallaro, L., & Liotta, A. (2022). Computer-aided diagnosis for breast cancer classification using deep neural networks and transfer learning.

Computer Methods and Programs in Biomedicine, *223*. https://doi.org/10.1016/j.cmpb.2022.106951

American Cancer Society. (2022). *Breast Cancer Facts & Figures 2022-2024*. https://www.cancer.org/content/dam/cancer-org/research/cancer-facts-and-statistics/breast-cancer-facts-and-figures/2022-2024-breast-cancer-fact-figures-acs.pdf

American Cancer Society. (2023). *American Cancer Society Recommendations for the Early Detection of Breast Cancer*. https://www.cancer.org/content/dam/CRC/PDF/Public/9671.00.pdf

Avcı, H., & Karakaya, J. (2023). A Novel Medical Image Enhancement Algorithm for Breast Cancer Detection on Mammography Images Using Machine Learning. *Diagnostics*, *13*(3). https://doi.org/10.3390/diagnostics13030348

Barrios, C. H. (2022). Global challenges in breast cancer detection and treatment. *Breast*, *62*, S3–S6. https://doi.org/10.1016/j.breast.2022.02.003

Heine, J., Fowler, E., Scott, C. G., Jensen, M. R., Shepherd, J., Hruska, C. B., Winham,

S. J., Brandt, K. R., Wu, F. F., Norman, A. D., Pankratz, V. S., Miglioretti, D. L., Kerlikowske, K., & Vachon, C. M. (2021). Mammographic variation measures, breast density, and breast cancer risk. *American Journal of Roentgenology*, *217*(2), 326–335. https://doi.org/10.2214/AJR.20.22794

Hemali, S., Smita, A., Oza, P., Tanwar, S., & Alkhayyat, A. (2023). Mammogram Pre- processing Using filtering methods for Breast Cancer Diagnosis. *International Journal of Image, Graphics and Signal Processing*, *15*(4), 44–58. https://doi.org/10.5815/ijigsp.2023.04.04

Islam, M. R., Rahman, M. M., Ali, M. S., Nafi, A. A. N., Alam, M. S., Godder, T. K., Miah, M. S., & Islam, M. K. (2024). Enhancing breast cancer segmentation and classification: An Ensemble Deep Convolutional Neural Network and U-net approach on ultrasound images. *Machine Learning with Applications*, *16*, 100555. https://doi.org/10.1016/j.mlwa.2024.100555

Kaosain Akbar, M. (2022). Breast Cancer Prediction using Principal Component Analysis with Logistic Regression. *International Journal of Advances in Engineering and Management (IJAEM)*, *4*, 1189. https://doi.org/10.35629/5252-041011891196

Khairnar, S., Thepade, S. D., & Gite, S. (2021). Effect of image binarization thresholds on breast cancer identification in mammography images using OTSU, Niblack, Burnsen, Thepade's SBTC. *Intelligent Systems with Applications*, *10*(11), 46. https://doi.org/10.1016/j.iswa.2021.20

Leutenegger, S., Chli, M., & Siegwart, R. Y. (2011). BRISK: Binary Robust invariant scalable keypoints. *International Conference on Computer Vision*, 2548–2555. https://doi.org/10.1109/iccv.2011.6126542

Loizidou, K., Elia, R., & Pitris, C. (2023). Computer-aided breast cancer detection and classification in mammography: A comprehensive review. In *Computers in Biology and Medicine* (Vol. 153). Elsevier Ltd. https://doi.org/10.1016/j.compbiomed.2023.106554

Obeagu, E. I., & Obeagu, G. U. (2024). Breast cancer: A review of risk factors and diagnosis. *Medicine (United States)*, *103*(3), E36905. https://doi.org/10.1097/MD.0000000000036905

Shubham, K., & Kamalraj, R. (2022). Breast Cancer Detection Using Machine Learning Algorithms. *International Journal of Advances in Engineering and Management (IJAEM)*, *4*, 987. https://doi.org/10.35629/5252-0403987994

Soliman, N. F., Ali, N. S., Aly, M. I., Algarni, A. D., El-Shafai, W., & Abd El-Samie,

F. E. (2021). An efficient breast cancer detection framework for medical diagnosis applications. *Computers, Materials and Continua*, *70*(1), 1315–1334. https://doi.org/10.32604/cmc.2022.017001

Sun, Z., Lyu, M., Li, J., Wang, Y., & Gao, X. (2022). A local-nonlocal mathematical morphology. *Neurocomputing*, *495*, 51–61. https://doi.org/10.1016/j.neucom.2022.04.113

Trayes, K. P., & Cokenakes, S. E. H. (2021). Breast Cancer Treatment. *American Family Physician*, *104*(2), 171–178. https://www.aafp.org/pubs/afp/issues/2021/0800/p171.pdf

World Health Organization. (2025). *Breast Cancer*. World Health Organization. https://www.who.int/news-room/fact-sheets/detail/breast-cancer

Yasiran, S. S., Salleh, S., & Mahmud, R. (2020a). Otsu and Mathematical Morphology for Breast Cancer Classification. *ASM Science Journal*. https://doi.org/10.32802/asmscj.2020.sm26(4.9)

Yasiran, S. S., Salleh, S., & Mahmud, R. (2020b). Standard Deviation Based Otsu for Breast Cancer Classification. *ASM Science Journal*. https://doi.org/10.32802/asmscj.2020.sm26(4.19)

This is an open access article under the CC BY-SA license (https://creativecommons.org/licenses/by-sa/4.0/).